AVS18-01 Validation of H-SAF Snow Products with Physically Based Snow Energy Balance Model Driven by Downscaled Reanalyses Data

Final report: Juan Ignacio López Moreno, Esteban Alonso, Aynur Şensoy, A. Arda Şorman

30/04/2020

Contents

Summary

Limited snow observations in many mountain areas of the world are an important limitation to properly quantify water stored in snowpacks and to predict runoff during the melting period. In this study we compare simulated snow from two procedures of dynamical downscaling of atmospheric models (WRF and ICAR) with snow water equivalent and snow cover area retrieved from H13 and H10 satellite products respectively. The comparison was made in the Upper Euphrates Basin (Karasu Basin) (10250 km^2) in the Eastern Turkey, headwater of the Euphrates River where snow plays a major hydrological influence. ICAR is a promising tool for downscaling climate models at very detailed resolution with a moderate computational cost. However in this study, the simulation performed at 2 km resolution showed important deficiencies to simulate temperature and precipitation over the region, leading to a marked underestimation of snowpack. WRF was run at 10 km resolution and satisfactorily reproduced observed temperature and precipitation in the study area. Daily SWE series were rather realistic, exhibiting a high interannual variability for 2008-2018 period. Derived daily snow cover area (SCA) highly matched with the SCA series retrieved from H10 product at 5 km, although WRF-SCA showed some small deficiencies explained by the lower spatial resolution and some snowfall events which were not properly captured. SWE generated by H13 product over the study area seems to present deficiencies in terms of not being able to reproduce the spatial and temporal variability of snowpack. Apparently H13 saturates at a value for the basin´s average close to 150 mm, while WRF often simulates values between 200 and 280 mm. H13 product has also imperfaction to reproduce SWE variations driven by elevation and general slope aspect.

1. Introduction

Despite the inherent interest of properly quantifying the water stored as snow in mountain areas, this is still a challenging task due to lack of in-situ observations in most of cold regions of the world. In addition, the high spatial variability and the very dynamical nature of snowpack, subject to fast changes during both the accumulation and the melting period, poses great difficulty to interpolate those measurements over complex topography and hence quantifying the volume of water stored in snowpack which will be available during the melting period. In this sense, remote sensing has meant a noticeable advance to map snow cover area, snow cover fraction and even snow water equivalent from Microwave radiometry (MW). EUMETSAT has a number of products derived from MW measurements sensitive to snow thickness and density. In particular, the product H13 – SN-OBS-4 have different quality depending on the surface being flat, forested or mountainous. The algorithm is based on assimilating MW brightness temperatures of several channels at frequencies with different penetration in snow, into a first-guess field built by the (sparse) network of stations measuring snow depth for flat areas, for mountainous areas snow depth measured at stations is not used directly in the algorithm. A full description of the product can be found in: http://hsaf.meteoam.it/documents/PUM/SAF_HSAF_PUM-13_1_0.pdf. However, quality of snow water equivalent has been shown to be very sensitive to abrupt topography and the existence of liquid water content within the snowpack that strongly affects the microwave backscattering. In the frame of the AVS18-01 activity we have compared the snow water equivalent (H13) and snow cover area from snow recognition products (H10) with dynamical downscaling of reanalysis atmospheric data coupled with a physically based land surface model, applied to the Upper Euphrates (Karasu) Basin in Eastern Turkey. We have applied the Weather Research and Forecast model (WRF) to create meteorological and snow fields at 10 km resolution for a wide area including most of Turkey, Middle East, Caucasus and Mesopotamia forced by ERA-5 that covers the whole Earth on a 30 km grid and resolve the atmosphere using 137 levels from the surface up to a height of 80 km. Over a smaller domain (Karasu Basin, 10250 km^2) we have run a relatively new downscaling approach to reduce the resolution from 10 to 2 km using the Intermediate Complexity Atmospheric Research model (ICAR, Guttman et al., 2016) that is promising to gain spatial resolution with a reduced computational cost.

Snow outputs from H13 and H10 are compared to snow simulations using WRF and ICAR over the Karasu Basin where in and around meteorological and snow observations are available, permitting to discuss the potential and limitations of each of the compared products.

2. Methodology of the climate and snow simulations

The Weather Research and Forecast model (WRF) (Skamarock et al., 2008) is a non-hydrostatic mesoatmospheric numerical model designed for both atmospheric research and operational forecasting applications. It is widely used as dynamical downscaling and data assimilation tool. To provide the WRF model with the initial and boundary conditions, we downloaded the ERA5 reanalysis data (Hersbach, 2016). The data was downloaded from the Climate Data Store (CDS) infrastructure in grib format. We used the CDS python API to configure the downloads. The download covered the area between the 42ºN,25ºE and 36ºN,47ºE in degrees longitude and latitude and the time ranges from 01-Jan-1999 to 01-Dec-2018 at an hourly timestep. Due to the long download time it was possible to find corrupted files inside the downloaded data due to instabilities in the connection. To automatically avoid this problem, we used the output of the g2print.exe utility provided by the WRF model assuming that the corrupted files will be not readable. Thus, if the g2print.exe utility failed, the downloaded file was removed and requested again from the CDS.

The meteorological fields were downloaded separately for the model levels and for the single levels. Thus, the requested fields for the single levels were; the mean sea level pressure, the surface pressure, the skin temperature, the 2 meter temperature, the 10 meter U wind component, the 10 meter V wind component, the 2 meter dewpoint temperature, the geopotential, the land-sea mask, the sea surface temperature, the snow depth, the soil temperature level 1 (0-7 cm), the soil temperature level 2 (7-28 cm), the soil temperature level 3 (28-100 cm), the soil temperature level 4 (100-289 cm), the volumetric soil water layer 1 (0-7 cm), the volumetric soil water layer 2 (7-28 cm), the volumetric soil water layer 3 (28-100 cm), the volumetric soil water layer 4 (100-289 cm) and the logarithm of surface pressure. Additionally, we have downloaded the following variables on the model levels: the geopotential, temperature, the U component of wind, the V component of wind and the specific humidity. The necessary meteorological fields to properly run WRF from the ERA5 reanalysis overcome by far the size a limit of the CDS downloads. Thus, we had to separate the download over several smaller request. The download was performed automatically using a bash script that automatically iterates over seven days ranges, changing the dates inside the python programs which perform the request to the CDS.

The WRF model is constituted by two well differentiated steps. These are the WRF Preprocessing System (WPS) and the WRF model itself. The main objective of the WPS is to design the domain configuration, unpack the grib files and integrate all this information into netcdf files to be used by

WRF. These tasks are performed through the geogrid.exe, ungrib.exe and metgrib.exe utilities. The WRF step has the objective of generate the vertical interpolation of the WPS outputs onto the domain coordinates and finally run the numerical simulation. This is done through the use of real.exe and wrf.exe utilities.

Some preprocess was necessary over the ERA5 downloaded data to make the format compatible with the WPS system. The ERA5 reanalysis has too many model levels to be stored in grib1 format, that is why the ERA5 is stored in grib2 format. This format is not compatible with the WPS utilities, without the use of several dependencies. Thus, it was necessary to make some changes in original grib2 files to make them compatibles with the WPS modules. The ecCodes software was compiled from source and used to modify the structure of the grib ERA5 data. The modifications allowed WPS to read the grib2 files, even it is not designed for it. Then, the modified grib files were linked to the WPS directory using the link_grib.csh utility provided by the WPS software.

At the WPS step, we configured the domain of the WRF simulation using the geogrid.exe utility. The static geographical fields used in geogrid.exe (sea-land mask, land use, topography, vegetation and soil categories, among others) were provided by default. The domain configuration was designed with the center at the 38ºN, 42ºE coordinates with 220 cells in the West - East axis and 150 cells in the North – South axis. The spatial resolution was set to 10km in a Lambert conformal projection. As a consequence of the great amount of timesteps caused by the hourly resolution of ERA5, all the following steps inside the WPS were performed iteratively in ranges of 200 days and 23 hours. That was necessary due to limitations in the number of timesteps in the WPS utilities. The iteration was designed using the python language, resetting the dates of the WPS namelist at each iteration. Thus, the ungrib.exe utility was run over the single levels grib files and the model level files separately to unpack the grib files into an intermediate file format. We generated two sets of intermediate WPS files, one for the single levels and the other from the model levels. Additionally, to the single levels and model levels intermediate files obtained by the data downloaded from the CDS, it was necessary to calculate the 3D pressure and geopotential on the same levels as the other atmospheric fields. Thus, the calc_ecmwf_p.exe utility was run, using the list of coefficients provided by the ERA5 documentation. Finally, to horizontally interpolate the meteorological fields into the WRF domain, the metgrid.exe utility was run over the intermediate single levels, model levels, new generated pressure files and geographical static fields to horizontally interpolate the meteorological fields to the model domain.

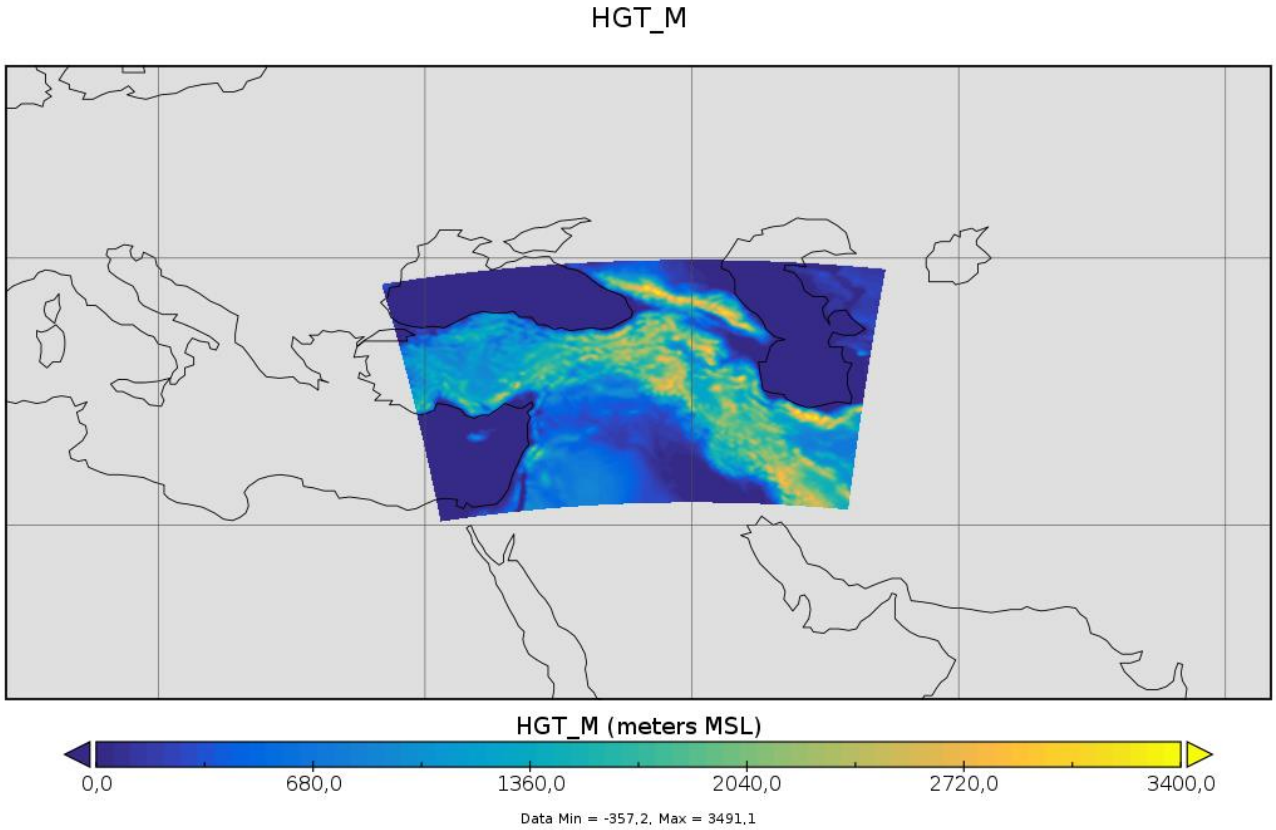

Figure 1: WRF simulation 10 km resolution domain

To generate the inputs files of WRF, we run the real.exe utility to perform the vertical interpolation of the metgrid.exe outputs, generating the boundary and initial conditions of WRF and checking the consistency of the metgrid.exe files. As the WRF step has some limitations in the number of timesteps, we repeat the same procedure as with the WPS step. Thus, we develop a python program that automatically handle the dates of the name list of WRF, dividing the task in smaller equally jobs of 200 days and 23h. Each real.exe task was submitted independently to different nodes of the supercomputing facilities of the Spanish Research Council at the same time to force to compute in parallel each time period, sharing each time period over 10 cores inside each node.

Finally, the WRF.exe utility was run over the outputs of real.exe, performing the numerical atmospheric simulation itself. Due to a limitation in timestep similar to the previous steps, we had to write a new python program to automatically handle the dates of the WRF namelist. At this step, more complexity is added, as the numerical simulation cannot be stopped as it dependent of the previous timestep calculations, while in the previous utilities each timestep can be computed independently. Thus, we have to force WRF to stop every 200h and 23h time period, and re-ran the simulation using the restart option of the WRF namelist. Thus, WRF generated a restart file at the

end of each time period to be reinitialized. The WRF simulation was parallelized between 200 cores in the supercomputing facilities of the Spanish Research Council.

The WRF simulation was configured following previous experiments, were the model has proven to provide reliable simulations of the winter precipitation over complex terrain (Ikeda et al., 2010; Rasmussen et al., 2011). Thus, the parametrization schemes used in WRF simulation include: the Thompson cloud microphysics scheme, for both shortwave and longwave radiations the NCAR Community Atmosphere Model (CAM) scheme is used, the land surface physics are solved by the Noah-MP scheme, the Mellor-Yamada-Janjic scheme for the planetary boundary layer and the Betts-Miller-Janjic scheme for deep and shallow convection. Noah-MP scheme for the land surface physics is particularly relevant in this study, as it has a three layers snowpack model with more realistic snow physics compared with other land surface models including: a thin surface layer, liquid water retention and refreezing, snowpack densification, sublimation and turbulent and radiative heat flux exchanges to and from snowpack with soil and plant canopy interactions. In addition, the spectral nudging technique was used to satisfy the large-scale features inside the domain. This forcing allows simulated large-scale fields advecting across the domain to remain consistent with the external dataset at the boundaries. The spectral nudging was applied in the upper levels, permitting the model to have its own dynamics inside the planetary boundary layer.

Then, a finer 2 km resolution ICAR (Intermediate Complexity Atmospheric Research model (Gutmann et al., 2016)) (Figure 2) simulation was nested inside the previous WRF simulation. ICAR is a quasi-dynamical downscaling model that uses simplified wind dynamics to perform high-resolution meteorological simulations 100 to 1000 times faster than a traditional atmospheric model. First, the WRF output had to be preprocessed to make it compatible with the ICAR model. Thus, we used the wrf2icar.sh batch script provided as a helper of the ICAR model. The primary reason for this script is to rotate the wind field into earth-relative coordinates instead of having them as model grid relative. In addition, it handles a number of issues to make the files smaller and more intuitive like some unit transformation or the computing of the geopotential height from the perturbation geopotential and the base-state geopotential WRF outputs. This utility uses the NetCDF Operators command line tool (NCO) to efficiently work with netcdf data. Thus, we previously had to compile from source the NCO tool with all of its dependencies in the supercomputing facilities of the Spanish Research Council to preprocess all the WRF output. Then, we ran the wrf2icar.sh over all the WRF outputs, after slight modifications of the code to make it compatible with the WRF version used in this study. Then, we designed the domain using the geogrid.exe utility of the WPS. Thus, the domain was designed with the center at the 39.66ºN, 40.65ºE coordinates with 200 cells in the North to South axis and 200 cells in the West to East axis.

The spatial resolution was set to 2 km in a Lambert conformal projection. As ICAR model has not MPI (Message Passing Interface) implemented yet, the parallelization of the simulation was performed in a single node of the supercomputing facilities of the Spanish Rearch Council performing the parallelization along its 32 processors. The model top was situated at 4150 m above the topography with 12 levels, using the default model levels height (Horak et al., 2019). The model configuration was selected as follows: the Thompson cloud microphysics scheme, the Noah land surface model and the Multidimensional Positive Definite Advection Transport Algorithm (MPDATA) for the advection. Convection schemes where not implemented for this simulation as they caused unstability problems in the model, probably as consequence of the high resolution. The radiative fluxes at the surface where the prescribed by WRF.

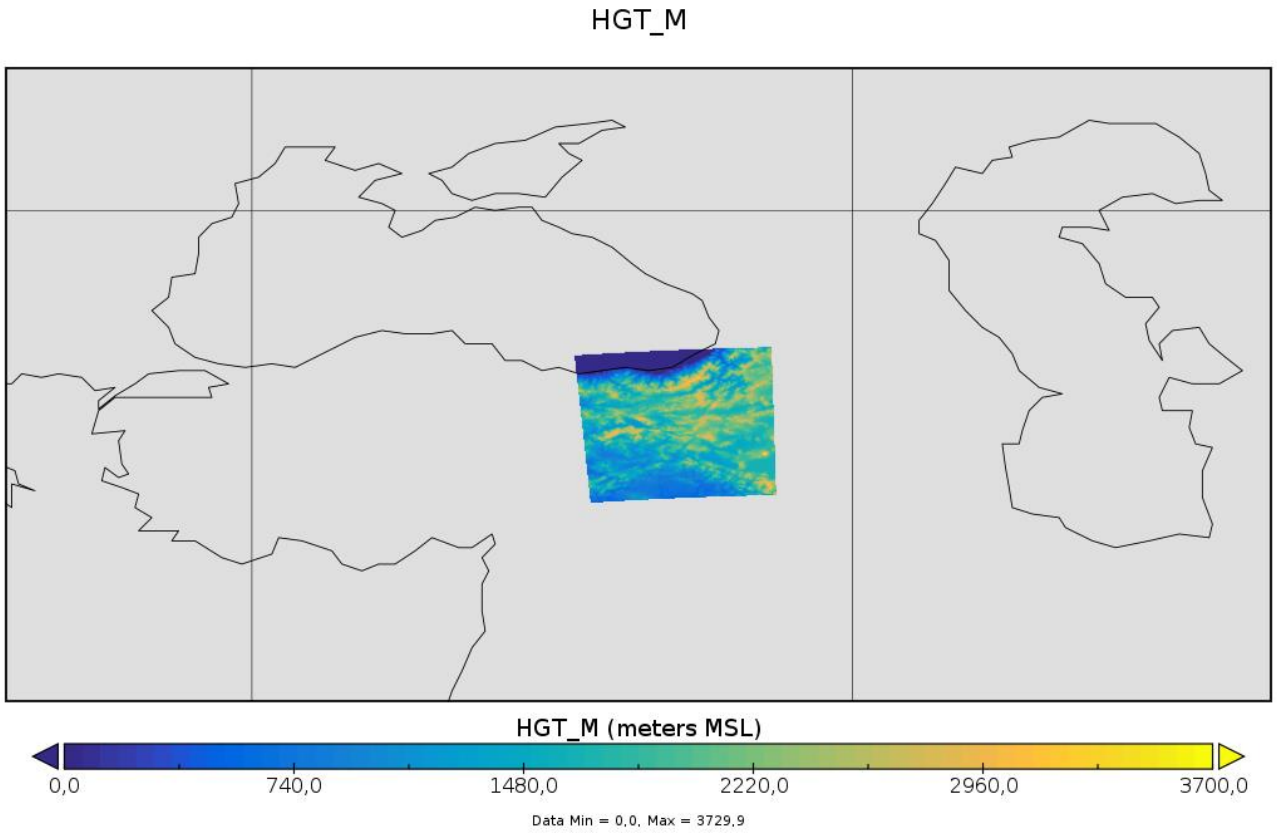

Figure 2: ICAR 2 km resolution simulation

3. Study area

The River Euphrates, the longest in southwest Asia (2700 km), is formed by the union of two major tributaries: the Karasu, which rises in the highlands of eastern Turkey, and the Murat, which originates north of Lake Van (Cullen and Menocal, 2000). The Euphrates Basin is largely fed from snow precipitation over the uplands of northern and eastern Turkey. About two-thirds of the precipitation occurs in winter, during which all precipitation falls as snow and which may remain

half of the year. This is followed by a sustained period of high flows during the spring resulting from melting of the snowpack. This not only causes extensive spring flooding, inundating large areas, but also the loss of much needed water during the summer season (Altınbilek, 2004). Karasu Basin, a sub-basin of the River Euphrates, is the test basin for this study. The region is mountainous and according to the long-term analysis of the hydrographs, snowmelt constitutes 60–70% of total annual streamflow volume. Most of the water that originates from snowmelt contributes to large reservoirs located on the River Euphrates in Turkey. The study area is basically the headwaters, Karasu basin, represented by the drainage area of stream gauging station 2119 The selected study area (Karasu Basin) is located within the longitudes 38°58′E to 41°39′E and latitudes 39°23′N to 40°25′N. It has a drainage area of 10,275 km^2 and ranges in altitude from 1125 to 3487 m (Figure 7). The main land cover types are pasture, agriculture and bareland.

4. Results

4.1 Capacity of WRF and ICAR to reproduce precipitation and temperature.

Figure 3 shows the evolution of observed temperature and simulated by WRF and ICAR in 2018 for meteorological observatories located within the domain shown in Figure 2. ICAR has shown clear deficiencies when reproducing temperatures. It is able to reproduce well the seasonal cycle and some of the most relevant temperature anomalies in the four observatories, but there is an obvious overestimation with respect to observations that in best case is close to 5ºC, but it can exceed 15ºC as happens in Hopa after April 2018. In contrast, WRF reproduces rather accurately the evolution of observed temperature with a Mean Bias Error oscillating between -0.75 and -1.9ºC, being the largest errors concentrated in few days of each data series. It is not observed any systematic bias in the observed errors although there is a dominance of WRF to slightly overestimate (warms) the simulated values.

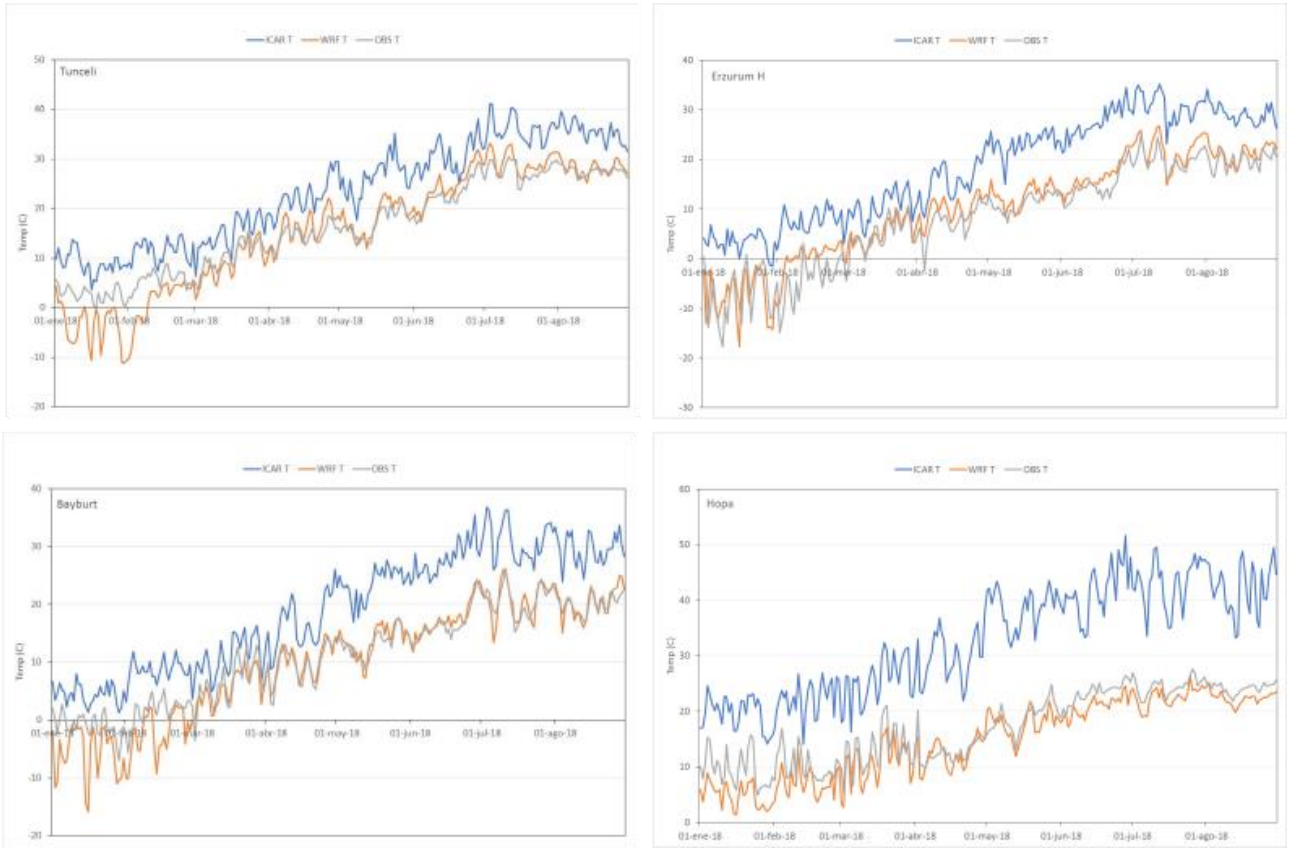

Figure 3. Evolution of observed and simulated daily temperature in 2018 by WRF and ICAR with meteorological observatories (Tunceli: 986 m a.s.l., Erzurum H: 1778 m, Bayburt: 1584 m, Hopa: 33 m)

Figure 4 shows the observed and simulated accumulated daily precipitation in the same four observatories. ICAR fails to reproduce adequately the observed precipitation, with clear underestimation of the observed values that is particularly evident in Erzurum and Hopa stations. WRF makes a much better work for reproducing precipitation, especially when data is considered until April that is the most relevant period for subsequent interpretations of the capability of WRF to simulate snowpack. Errors in Tunceli and Hopa are below 20% if the period from January to April is considered. It is interesting to note that in both Erzurum and Bayburt overestimates the observed values, however a careful consideration must be done in both places since these locations are above 1500 m a.s.l. and much of the winter precipitation falls as snow, which could make that real precipitation could be closer to the simulated one due to undercatch (Kochendorfer, in press). The better capability to obtain realistic fields of precipitation by meteorological model in cold regions has been previously stated for other areas of the world.

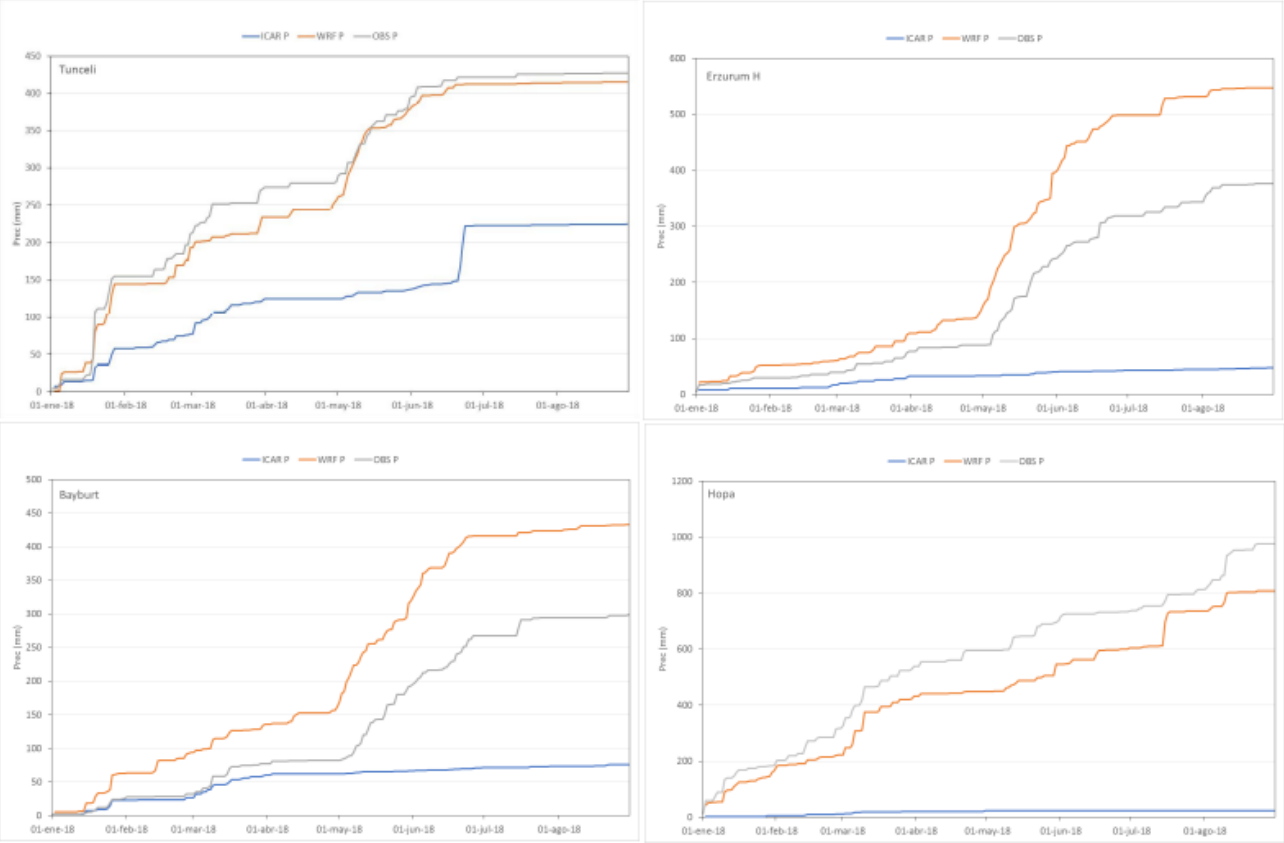

Figure 4. Evolution of observed and simulated daily accumulated precipitation of WRF and ICAR in 2018 in four meteorological observatories (Tunceli 986 m a.s.l., Erzurum H: 1778 m, Bayburt: 1584 m, Hopa: 33 m).

In summary, despite ICAR has been run at higher spatial resolution (2 km) and topography is much better represented, results evidence a very poor capability to reproduce temperature and precipitation fields observed in the study area. The simplified dynamical solver to reduce the computational demand together the topographic complexity and the mountainous character of the boundary area are plausible explanations of the poor results obtained. This results remarks the difficulty to select correctly the parameters of the linear wave theory used by ICAR, that has proved to be very sensitive to such configuration (Horak et all. 2019). WRF run at 10 km resolution reproduces reasonably well the observed fields of temperature and precipitation and it results a promising tool to simulate snowpack over the study area.

4.2 Comparison of snowpack characteristics retrieved from remote sensing data and atmospheric simulations.

According to the analysis of basin average snow water equivalent derived from WRF, ICAR and H13 (Figure 5) in between 2012-2018 water years, ICAR results are totally different compared to the other two as the values given in the second vertical axis. Concerning the temperature and precipitation analysis, the results with lower SWE values can be expected. In comparison of SWE results of WRF and H13, even though there is a relatively high consistency between these two for the last three years, theyare different for the previous three years. H13 product provides relatively homogeneous results over the basin (Figure 6) and it seems as it saturates at some threshold that makes that average SWE for the basin not exceed a certain limit of SWE, next to 140 mm, value over the years (Figures 5 and 6). On the other hand, WRF simulates average values for the basin that exceed 250mm, and the spatial distribution seems to be varied over the basin consistent with the topography (Figure 7). As result the SWE analysis provides different data range for different years. Concerning the very dry period in 2014 where the runoff values and snow observations indicates lowest values of last years, WRF SWE results verify this condition in Figure 4, while H13 provides SWE results similar to the other years. Since, the basin area is not fully screened by the satellite some days, those days are eliminated for H13 product. Having a better areal resolution is also an advantage for WRF result. In addition, hydrological information of the Karasu basin reveals that spring runoff is largely influenced by snowmelt also exhibits a high interannual variability, oscillating the average runoff from March to May between 50 and 250m^3s^{-1}. Such variability is very difficult to explain under the very constant peak SWE obtained from H13 product. However, interannual variability of Peak SWE simulated by WRF explains a 58% of the variance shown by spring runoff (analysis not shown in this report).

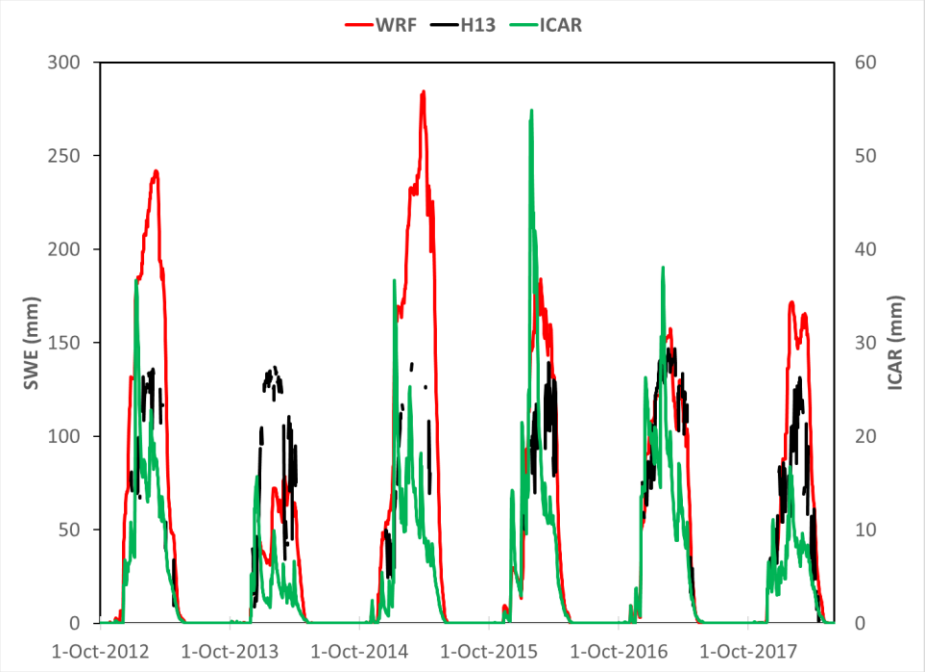

Figure 5. Evolution of basin average snow water equivalent from WRF, ICAR and H13 in between 2012-2018.

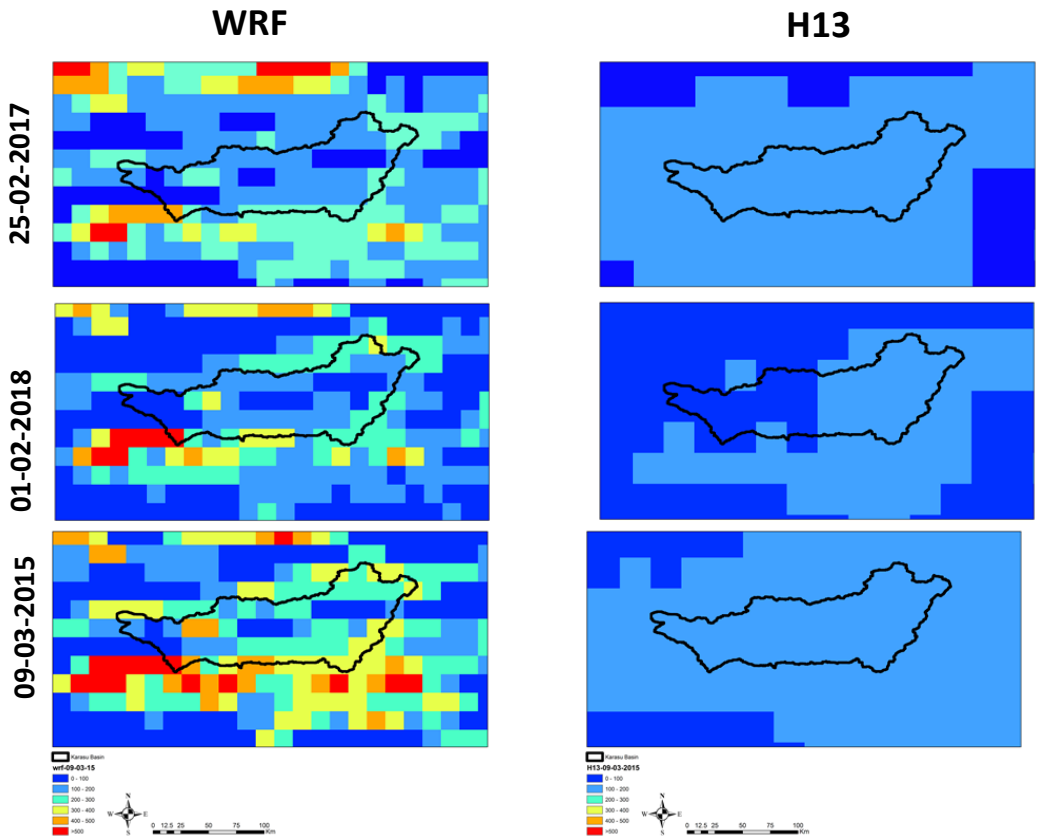

Figure 6. Visual comparison of SWE derived from WRF and H13 for Karasu Basin a) 25 Feb 2017 b) 01 Feb 2018 c)09 Mar 2015

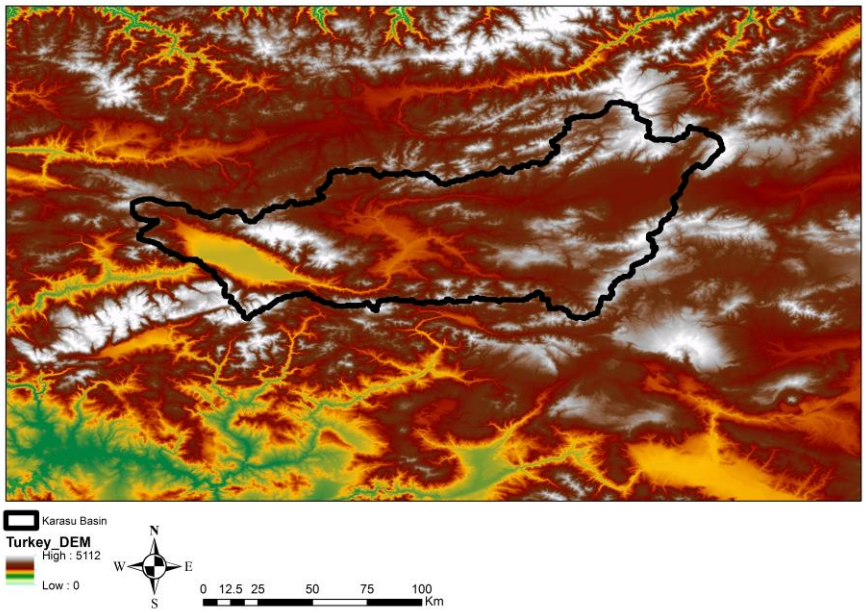

Figure 7. Digital elevation model of the basin

Another comparison is done for snow cover depletion of the basin as time series for the water years 2014-2018 in Figure 8. WRF SWE maps were converted to snow covered extent maps with some trials of SWE thresholds, the best results are achieved by 10 mm. Then, snow covered extent values were extracted from WRF and they were compared with that of H10 snow products. The consistencies between the values are as high as NASH of 0.95 for the last three years and 0.65 for the first year of analysis where WRF overestimates the snow cover during the melting period. The largest differences were observed during isolated events in the accumulation period (i.e. 2015-15 and 2016-17). Such deviations are likely associated to the different resolution of the two products, and also the isolated snowfall events that are not properly captured by WRF, or they are captured but with a biased snowline. These events do not affect to the overall estimation of the annual duration of the snowpack._Snow cover extent maps are also compared for two dates with less or without snow cover in Figure 9.

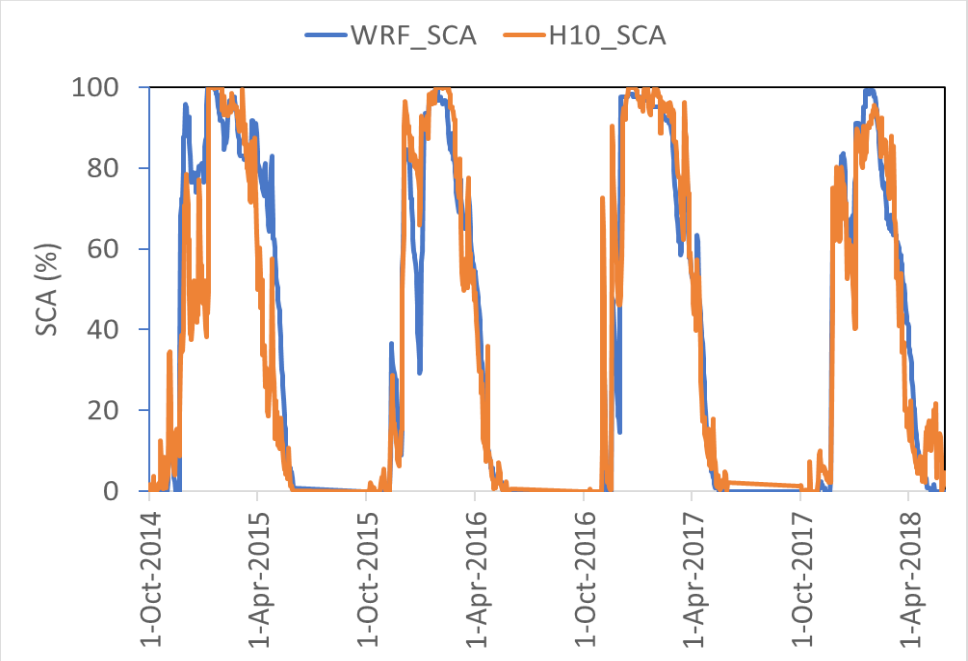

Figure 8. Evolution of basin average snow covered area from WRF and H10 in between 2014-2018.

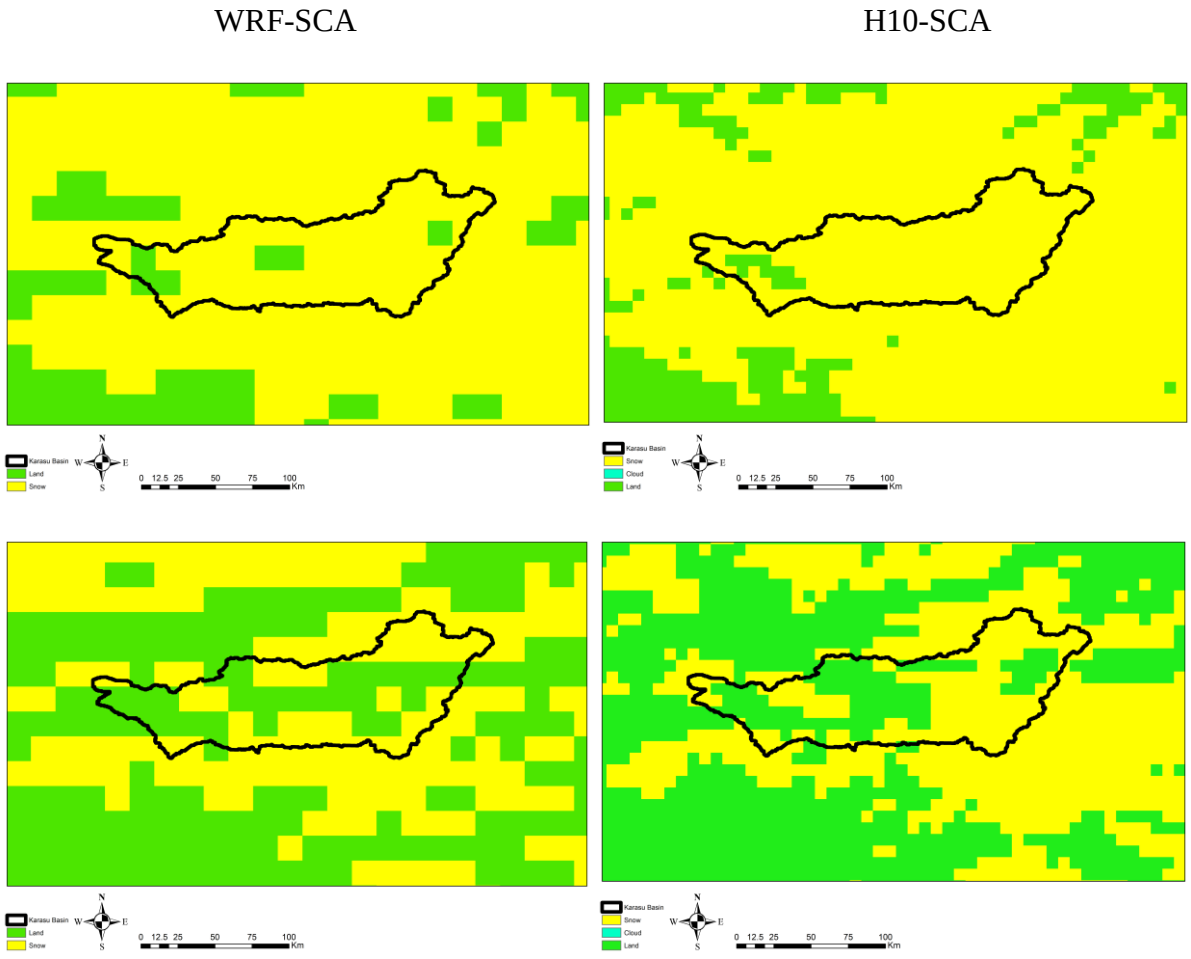

Figure 9. Visual comparison of SCA derived from WRF (left panels) and H10 (right panels) for Karasu Basin a) 25 Feb 2017 b) 29 Mar 2017

5. Conclusions

WRF has been used to satisfactorily downscale meteorological fields from ERA 5 reproducing adequately observed precipitation and temperature data over the study area. However, the attempt to gain spatial resolution with ICAR failed with clear overestimation of temperature in most of the observatories, and also a marked underestimation of precipitation. Such biases explain very low snow water equivalent (SWE) values simulated by ICAR over the Karasu Basin.

SWE values retrieved by H13 over the Karasu basin look tricky, showing a threshold close to 150 mm from which H13 saturates or simply is assigned when snowpack is present, making that retrieved maximum annual SWE was almost identical every year of the study period (2012-2018). At the same time, the distributed values exhibit little variability, with relatively less response to general slope aspect or elevation variation over the basin. SWE simulated from WRF at 10 km looks consistent with the high interannual variability and also there is a good agreement between the daily series of snow cover area derived from WRF and the ones derived from H10 product. However, H10 has the advantage of a finer resolution (5 km). SWE derived from WRF has been shown a good predictor of spring runoff over the Karasu Basin (explaining almost 60% of the observed variance).

REFERENCES:

Altinbilek, D.H. (2004). Development and management of the Euphrates–Tigris basin. International Journal of Water Resources Development, 20(1), 15–33. doi:10.1080/07900620310001635584

Cullen, H.M., & Demenocal, P.B. (2000). North Atlantic influence on Tigris–Euphrates streamflow. International Journal of Climatology: A Journal of the Royal Meteorological Society, 20(8), 853-863.

Gutmann, E., Barstad, I., Clark, M., Arnold, J., Rasmussen, R. (2016). The Intermediate Complexity Atmospheric Research model (ICAR). J. Hydrometeorol. 17, 957–973. https://doi.org/10.1175/JHM-D-15-0155.1

Hersbach, H. (2016). The ERA5 Atmospheric Reanalysis., in: Agufm. pp. NG33D-01.

Horak, J., Hofer, M., Maussion, F., Gutmann, E., Gohm, A., Rotach, M.W., 2019. Assessing the added value of the Intermediate Complexity Atmospheric Research (ICAR) model for precipitation in complex topography. Hydrol. Earth Syst. Sci. 23, 2715–2734. https://doi.org/10.5194/hess-23-2715-2019.

Ikeda, K., M. Steiner, and G. Thompson, 2017: Examination of mixed-phase precipitation forecasts from the High-Resolution Rapid Refresh model using surface observations and sounding data. Wea. Forecasting, 32, 949–967

Kochendorfer, J., M.E. Earle, D. Hodyss, A. Reverdin, Y. Roulet, R. Nitu, R. Rasmussen, S. Landolt, S. Buisan, and T. Laine (*in press)*. Undercatch adjustments for tipping bucket gauge measurements of solid precipitation. J. Hydrometeor., *in press*, https://doi.org/10.1175/JHM-D-19-0256.1

Rasmussen R, Ikeda K, Liu C, Gochis D, Clark M, Dai A, Gutmann E, Dudhia J, Chen F, Barlage M, Yates D, Zhang G (2014). Climate change impacts on the water balance of the Colorado headwaters: High-resolution regional climate model simulations. J Hydrometeorol 15:1091–1116

Skamarock, W.C., Klemp, J.B., Dudhia, J.B., Gill, D.O., Barker, D.M., Duda, M.G., Huang, X.-Y., Wang, W., Powers, J.G. (2008). A description of the Advanced Research WRF Version 3, NCAR Technical Note TN-475+STR. Tech. Rep. 113. https://doi.org/10.5065/D68S4MVH.